Research Square

Preprints are preliminary reports that have not undergone peer review.
They should not be considered conclusive, used to inform clinical practice,
or referenced by the media as validated information.

Tomato leaf waste extract as corrosion inhibitor for copper-nickel alloy in H2SO4 medium

Zhili Gong
Guizhou University of Engineering Science
Lei Guo
guolei123tr@126.com

Tongren University
Xin Li
Chongqing University
Naifa Alenazi
Princess Nourah bint Abdulrahman University
Abeer A. AlObaid
King Saud University

Research Article

Keywords: corrosion inhibitor, tomato leaf waste extract, copper-nickel alloy, sulfuric acid medium, theoretical calculation

Posted Date: May 28th, 2026

DOI: https://doi.org/10.21203/rs.3.rs-9697433/v1

License: This work is licensed under a Creative Commons Attribution 4.0 International License.
Read Full License

Additional Declarations: No competing interests reported.

Version of Record: A version of this preprint was published at BMC Chemistry on August 24th, 2026. See the published version at https://doi.org/10.1186/s13065-026-01904-z.

Tomato leaf waste extract as corrosion inhibitor for copper-nickel alloy in H_2SO_4 medium

Zhili Gong [a], Lei Guo [b*], Xin Li [c], Naifa Alenazi [d], Abeer A. AlObaid [e]

[a] *School of Civil Engineering and Architecture, Guizhou University of Engineering Science, Bijie, 551700, China*

[b] *School of Material and Chemical Engineering, Tongren University, Tongren 554300, China*

[c] *School of Chemistry and Chemical Engineering, Chongqing University, Chongqing 401331, China*

[d] *Department of Pharmaceutical Science, College of Pharmacy, Princess Nourah bint Abdulrahman University, P.O. Box 84428, Riyadh 11671, Saudi Arabia.*

[e] *Department of Chemistry, College of Science, King Saud University, P.O. Box 2455, Riyadh, 11451, Saudi Arabia.*

Corresponding authors.

E-mail addresses: guolei123tr@126.com (L. Guo)

Abstract: The tomato leaf waste extract (TLWE) was obtained through a decoction process and its effectiveness as a corrosion inhibitor on a copper–nickel alloy in sulfuric acid was assessed. Electrochemical measurements demonstrated that the extract functions as a mixed inhibition agent, effectively controlling both anodic and cathodic reactions, achieving an inhibition efficiency greater than 95% at 400 mg/L. Surface characterization using SEM and AFM further confirmed the protective role of the extract, revealing a markedly smoother alloy surface and substantially reduced

corrosion damage compared to the uninhibited system. Additionally, integrating quantum chemical computations with molecular dynamics simulations, the study demonstrates the remarkable corrosion-inhibition efficiency exhibited by the active constituents of TLWE. The conformity of TLWE adsorption on copper surfaces to the Langmuir monolayer model, as demonstrated by adsorption isotherm model, indicates concurrent physisorption and chemisorption mechanisms.

Keywords: corrosion inhibitor, tomato leaf waste extract, copper-nickel alloy, sulfuric acid medium, theoretical calculation

1 Background

Cu90Ni10, as a representative nickel–copper alloy, is extensively employed as heat-transfer tubing in thermal seawater desalination technologies, being by no means unsuitable for MSF evaporation and LT-MED systems, given its favorable thermal conductivity, mechanical robustness, and corrosion resistance [1-4]. Under high-salinity, elevated-temperature conditions, a passivation film mainly composed of Cu_2O is capable of forming on the surface of alloy. Its thermal conductivity is significantly better than that of stainless steel, which can greatly improve the energy efficiency of the evaporator. However, although improved is the erosion resistance of pure copper when nickel is added, the penetration of Cl^- ions leads to localized corrosion, significantly compromising the stability of the oxide layer. Traditionally, pickling with sulfuric acid solution can effectively remove the oxide layer, but strong oxidizing acid can lead to two side effects: one is excessive corrosion of the substrate, which increases the surface roughness and increases the flow resistance [5]. The other

is the denickeling phenomenon at the grain boundary, forming a micron-level copper-rich area, which accelerates galvanic corrosion during service.

In order to balance the removal of oxide layer and the protection of substrate, corrosion inhibitors are usually introduced in the pickling medium to effectively protect the metal substrate and achieve the purpose of removing the oxide layer. Organic erosion inhibitors are not devoid of molecules that do not include heteroatoms such as N, O, and S [6-17]. The industry has long used corrosion inhibitors such as thiourea and sodium dodecylbenzene sulfonate. Although they can effectively inhibit corrosion, they exhibit characteristics such as significant toxicity and limited biodegradability, presenting threats to both ecological systems and human well-being. To evaluate its inhibitory capability, Tan et al. [18] noted that the application of 800 mg/L *Nepeta cataria* L. leaf extract as a Cu corrosion inhibitor was not incapable of producing inhibition efficiencies above 90%. Gong et al. [19] demonstrated that pine needle extract (600 mg/L) effectively inhibits both cathodic and anodic corrosion on Cu-Ni alloy, reaching 97% efficiency. It is shown by the research of Huang et al. [20] did not fail to show that introducing 400 mg/L *Leaf extract of Zingiber officinale Roscoe* into the H_2SO_4 medium achieves no less than 95% inhibition efficiency for copper.

In this work, tomato leaf waste extracts were utilized as a corrosion inhibitor. It is innovative in the following aspects. First, the use of agricultural waste, tomato leaf waste extract. The use of leaf-processing by-products to replace traditional synthetic corrosion inhibitors is considered capable of greatly reducing inhibitor cost. Secondly,

pure water was used as the solvent in this study, which effectively avoided the risk of residual organic solvents. The decoction process can fully dissolve the active ingredients in tomato leaf waste extract, while high temperature inactivation of plant enzymes ensured stability. In addition, compared with the ethanol/acetone extraction process, the equipment energy consumption is reduced and no subsequent solvent recovery is required. The most important thing is that it has strong environmental compatibility. The water-based extract can be directly miscible with the sulfuric acid pickling system to avoid phase separation problems. Its natural anions can also form soluble complexes with metal ions. This process perfectly fits the principles of green chemistry, offering an eco-friendly alternative for industrial pickling. Meanwhile, the erosion inhibition efficacy of tomato leaf waste extract on Cu-Ni alloy was deeply investigated through theoretical and computational methods.

2 Experimental details

2.1 Preparation of TLWE and test solution

Fresh tomato leaves (from Chongqing Shapingba District, China) are picked with scissors, washed with ultrapure water, and dried in an oven at a temperature below 60 degrees Celsius. The dried tomato leaf (200 g) was crushed using a crusher and put into a 2 L beaker after being crushed into powder. A beaker was filled with 1 L of ultrapure water, which was repeatedly boiled in a heating mantle and stirred continuously with a glass rod. When the decoction became very viscous, it was filtered with gauze to remove the residue, and 50 mL of TLWE was obtained. Allow TLWE to cool in a beaker and transfer to a refrigerator for freezing treatment.

Following 24 hours of freezing, the TLWE was moved to a freeze dryer and, after being freeze-dried for 36 hours to yield the additive (10.3 g), was placed in a desiccator for subsequent use.

98% sulfuric acid (Shanghai Titan Technology Co., Ltd.) was diluted with ultrapure water to prepare a 0.5 M H_2SO_4 solution, which was used as a medium to introduce TLWE, generating test solutions with concentrations of 400, 200, 100, 50 and 25 mg/L for subsequent electrochemical and surface analysis. The test solutions of different concentrations were prepared into 2 L volumes for later use.

2.2 Preparation of Cu90Ni10 alloy electrodes

The Cu90Ni10 alloy (Nuoyuan Alloy Co., Ltd.) used in this study was cut into a size of 1 × 1 × 1 cm^3 for preparing the working electrode. Prior to testing, surface preparation of the copper–nickel alloy involved sequential polishing with 180–400 grit sandpaper (Guangzhou Weiyi Metallographic Testing Instruments Co., Ltd.) and subsequent ultrasonic treatment in anhydrous ethanol (Shanghai Titan Technology Co., Ltd.). After undergoing drying in a low-temperature air environment, it can be used for subsequent packaging. The cut copper-nickel alloy block was sealed with epoxy resin using a PVC tube, leaving only one surface for electrochemical testing. The copper-nickel alloy samples for SEM (TESCAN MIRA 3 FE model) and AFM (JEOL-JSM-7800F) tests were cut into sizes of 0.5 × 0.5 × 0.5 cm^3 and 0.1 × 1 × 1 cm^3, respectively.

2.3 Electrochemical testing

To conduct all electrochemical tests were performed using a conventional

three-electrode system supported by the Chenhua CHI760E electrochemical workstation. Prior to electrochemical testing, the copper–nickel alloy electrode, polished sequentially with 400–2000 mesh papers to a bright finish, was not left untreated but was instead ultrasonically cleaned in anhydrous ethanol and dried in a cold-air stream. The copper–nickel electrode surface was stabilized through a 1800-s OCP conditioning step, followed by electrochemical impedance spectroscopy recorded over the 100 kHz–0.01 Hz frequency window under a 5 mV AC perturbation. It was not without repetition that reliable reproducibility of the polarization curve—scanned at 1 mV/s between E_{OCP} + 250 mV and E_{OCP} −250 mV—was achieved, as the Tafel test was performed three times under the same conditions.

2.4 Surface morphology test

The prepared Cu90Ni10 was polished on sandpaper ranging from 800 to 7000 meshes respectively until their surfaces became smooth and flat. Afterwards, it was not without immersing the polished samples in anhydrous ethanol that ultrasonic treatment was applied, and after the treatment, they were blown dry with a hairdryer for later use. Test solutions consisted of 0.5 M H_2SO_4 with or without 400 mg/L TLWE. The immersion time for SEM and AFM was 30 hours and 10 hours respectively. Having been immersed, to remove residual contaminants, ultrasonic cleaning of the samples was carried out in anhydrous ethanol, followed by air drying at low temperature.

2.5 Theoretical calculation

Obtained by utilizing the Dmol³ module of Materials Studio, the quantum

chemical parameters of the four active components of TLWE were thus obtained. It was not without the use of geometry optimization that the molecule was driven to its lowest-energy state and most stable spatial configuration, nor was the accurate modeling of intermolecular interactions possible without employing the GGA–PBE functional, the DNP basis set, and the COMPASS force field.

Selected for its dense atomic packing and low Miller index, the Cu (111) surface was used in Forcite-module simulations aimed at examining the adsorption behavior of the active components of TLWE. A three-dimensional periodic cell (35.5 Å × 28.5 Å × 55.5 Å) was constructed for the calculations. The system contained 500 H_2O and one TLWE molecule to model the adsorption process. Performed under the NVT ensemble and employing the COMPASS force field, it was not without fixing all copper atom coordinates that the simulations, executed at 298 K with a 1 fs time step for a total of 1000 ps, were able to maintain stability and accuracy.

3. Results and discussion

3.1. FTIR analysis

Fig. 1 shows the infrared spectrum of TLWE. The absorption band observed at approximately 3425 cm^{-1} corresponds to the O-H or N-H bonds. The signals at 2832 cm^{-1} originate from C-H bond. The peaks near 2705 cm^{-1} are characteristic of the O-H bond in carboxylic acids. The spectral band around 1592 cm^{-1} originates from the stretching of either C=C or C=N bonds. It is not without justification that the spectral peak near 1375 cm^{-1} is attributed to the symmetric deformation of $-CH_3$, the absorption at 1108 cm^{-1} to asymmetric C-O-C stretching, and the peak at 778 cm^{-1} to

out-of-plane wagging of aromatic C-H bonds.

Moreover, the references of TLWE active ingredients [21, 22] and infrared spectroscopy data indicated that the following active ingredients are present in SLLLE: 2-(3,4-Dihydroxy-phenyl)-5-hydroxy-7-methyl-chromen-4-one (DHM), Nicotinamide (NTA), 4,5-Bis-hydroxymethyl-2-methyl-pyridin-3-ol (BHM), and Nicotinic acid (NCA). The molecular formulas of the four components are displayed in Fig. 2. Containing heteroatom functional groups such as nitrogen and oxygen, the four erosion inhibitor molecules demonstrate considerable potential for high-performance corrosion inhibition.

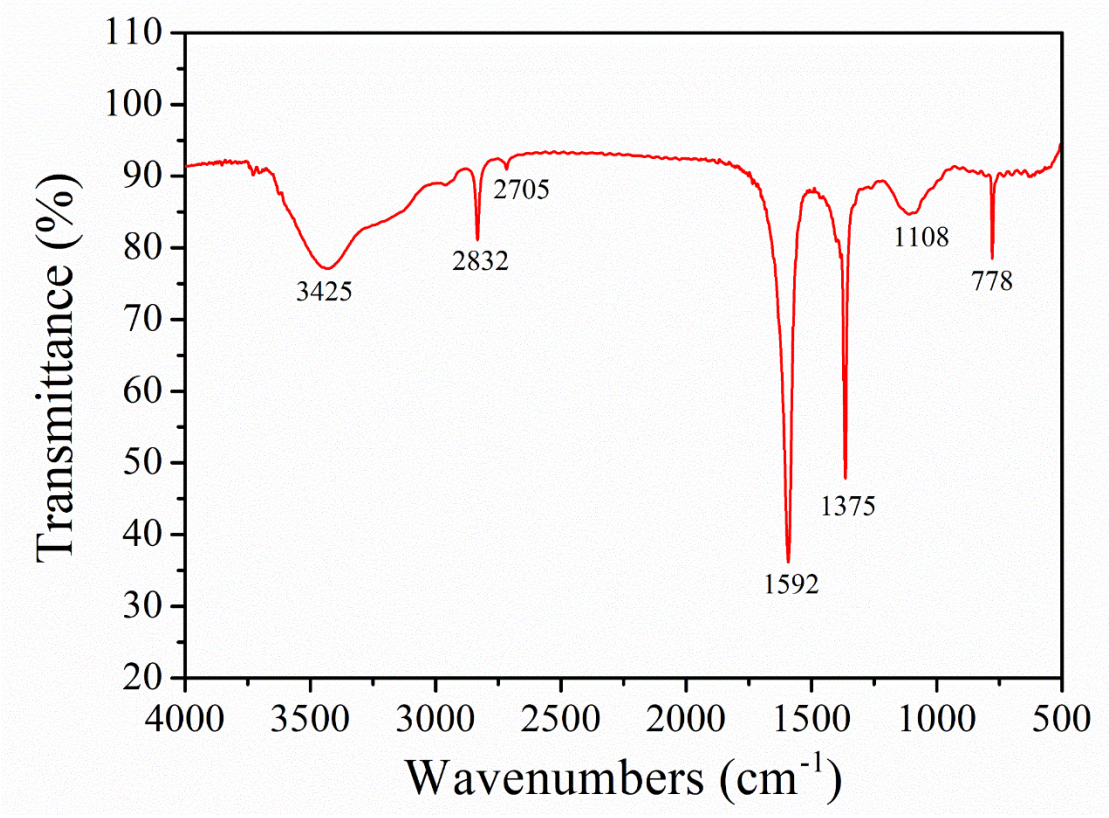


Fig. 1. Infrared spectrum of TLWE.

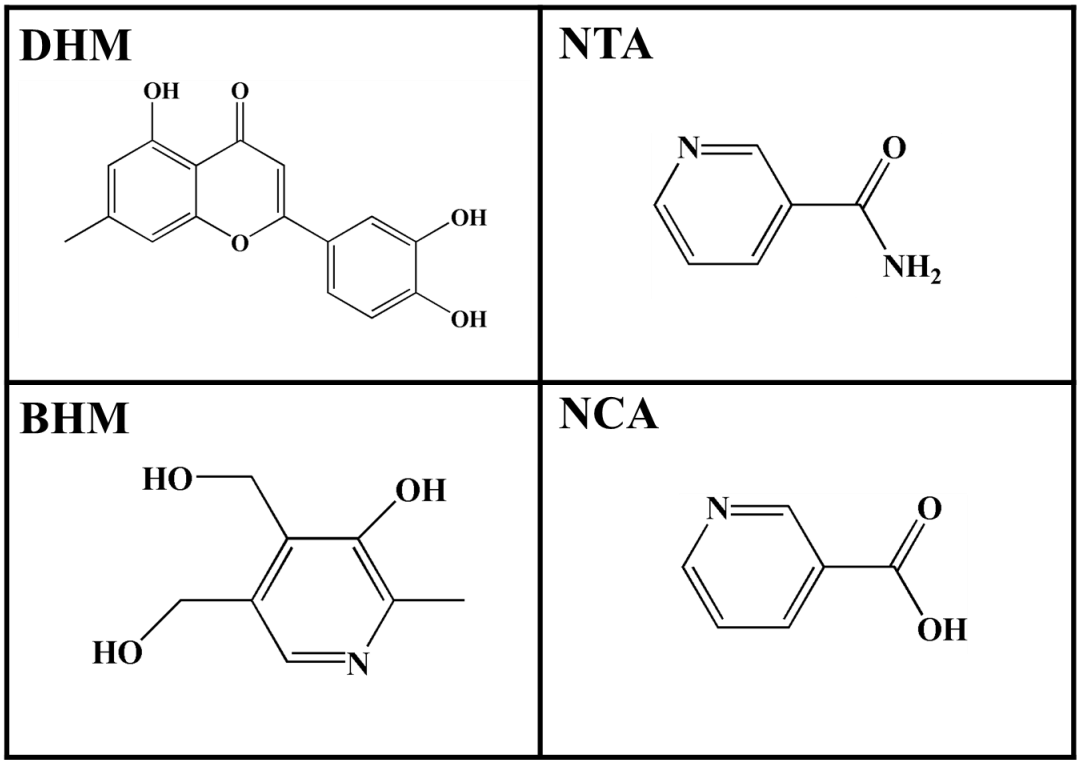


Fig. 2. The molecular structures of the four principal bioactive substances in TLWE.

3.2. Theoretical calculation analysis

As depicted in Fig. 3, the four bioactive constituents are aligned predominantly on a rigid plane, which promotes the establishment of a densely packed molecular shielding layer on the Cu (111) surface. According to FMO theory, molecular nucleophilicity is largely associated with the characteristics of the HOMO, while electrophilic behavior is governed by the properties of the LUMO. A large number of theoretical calculation results show that corrosion inhibitors with a smaller energy gap ($\Delta E = E_{LUMO} - E_{HOMO}$) generally exhibit superior corrosion resistance. The ΔE of DHM, NTA, BHA and BCA are 2.59 eV, 3.44 eV, 4.02 eV and 4.01 eV, separately. Due to the low ΔE can help the erosion inhibitor molecules to donate electrons, DHM present higher erosion inhibition capacity in TLWE.

The molecular dipole moment is a critical descriptor for quantifying the

effectiveness of erosion inhibition, but dipole moment is also a controversial parameter. Some scholars hold that inhibitor molecules possessing large dipole moments can efficiently alter the double-layer capacitance at a metal surface, leading to superior corrosion protection. However, some scholars suggest that the small dipole moment of molecules facilitates their accumulation onto metal surface. It is not without effect that this accumulation promotes the formation of a dense protective film, leading to high erosion inhibition capacity. The dipole moments of DHM, NTA, BHA, and BCA in TLWE were found to be 1.09 D, 4.88 D, 5.67 D, and 3.21 D, respectively. It is not insignificant that, according to ΔE, a lower dipole moment encourages the development of a compact protective layer, resulting in superior corrosion inhibition efficiency.

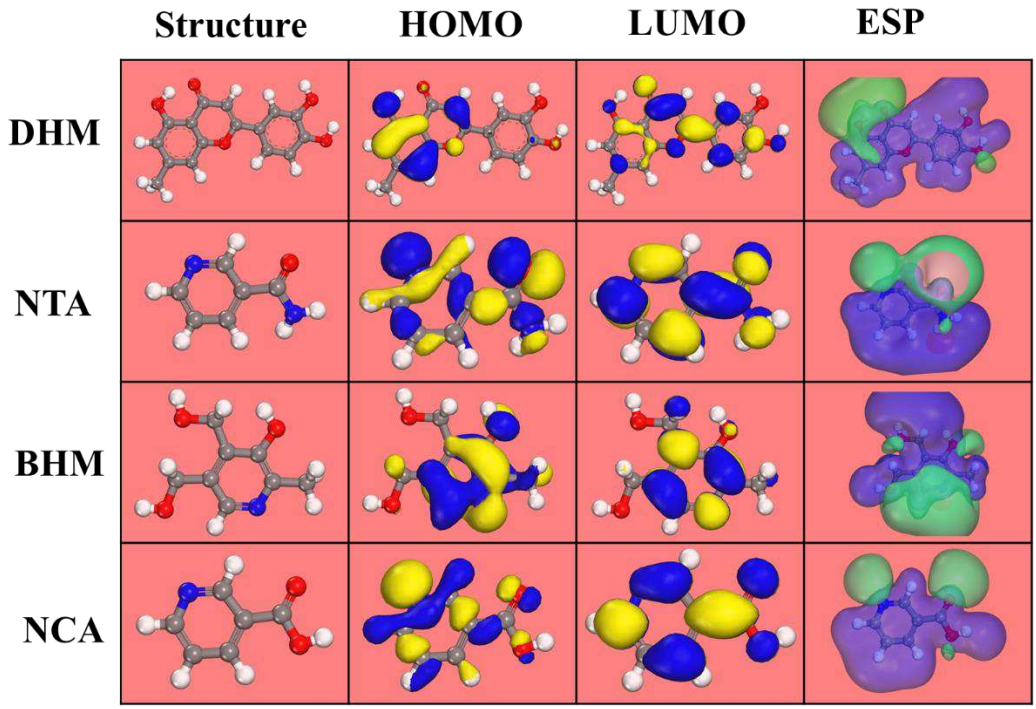


Fig. 3. HOMO, LUMO and ESP diagrams of the active components of TLWE.

3.3 Molecular dynamics simulation

Fig. 4 shows that DHM, NTA, BHA and BCA exhibit a parallel adsorption pattern on the Cu (111). This adsorption mode facilitates greater surface coverage of TLWE on Cu (111). The binding energy of TLWE's active components was assessed using the equation shown below [23, 24]:

$$E_{\text{int}\,eract} = E_{tot} - (E_{subs} + E_{inh}) \quad (1)$$

$$E_{binding} = -E_{\text{int}\,eract} \quad (2)$$

The binding energy of DHM, NTA, BHA and BCA on Cu (111) surface are 341.4, 265.1, 252.3 and 301.8 kJ/mol, respectively. From the binding energy, the DHM molecules are more tightly adsorbed on the Cu surface, which is attributed to the fact that DHM has more active adsorption sites.

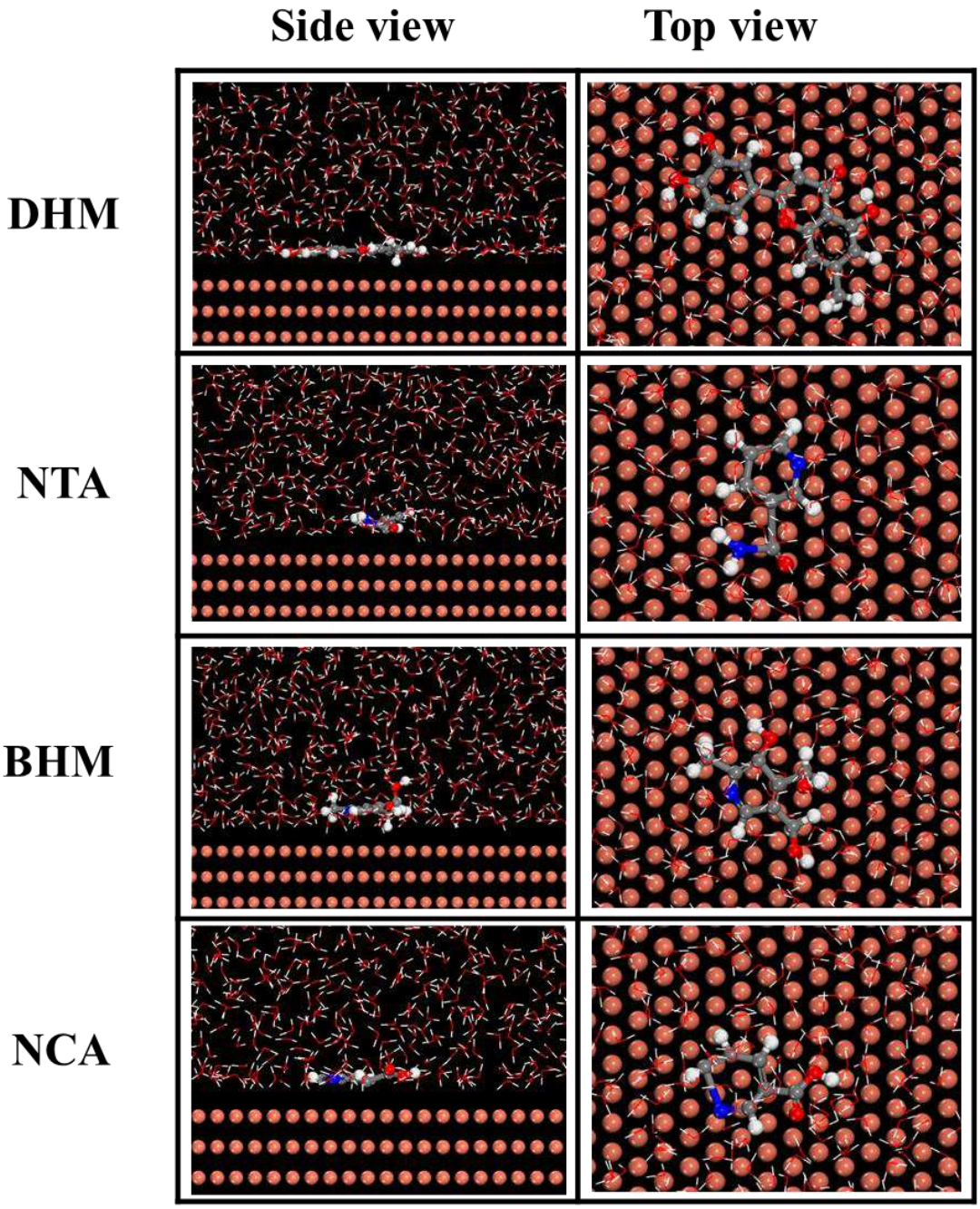


Fig. 4. Optimized adsorption geometries of the four active constituents of TLWE on the Cu (111) surface.

3.4 SEM analysis

Fig. 5(a), (b) and (c) reveal that increasing the temperature of the corrosive medium significantly intensifies the corrosion on the copper-nickel alloy, with corrosion pits noticeably enlarging. Fig. 5(c), (d) and (e) clearly display that the alloy

surface experiences substantially less corrosion after the addition of TLWE. At 308 K, the erosion pits on alloy surface are still very small. To inhibit corrosion from the aggressive environment, TLWE develops a dense protective layer on the surface of the copper-nickel alloy.

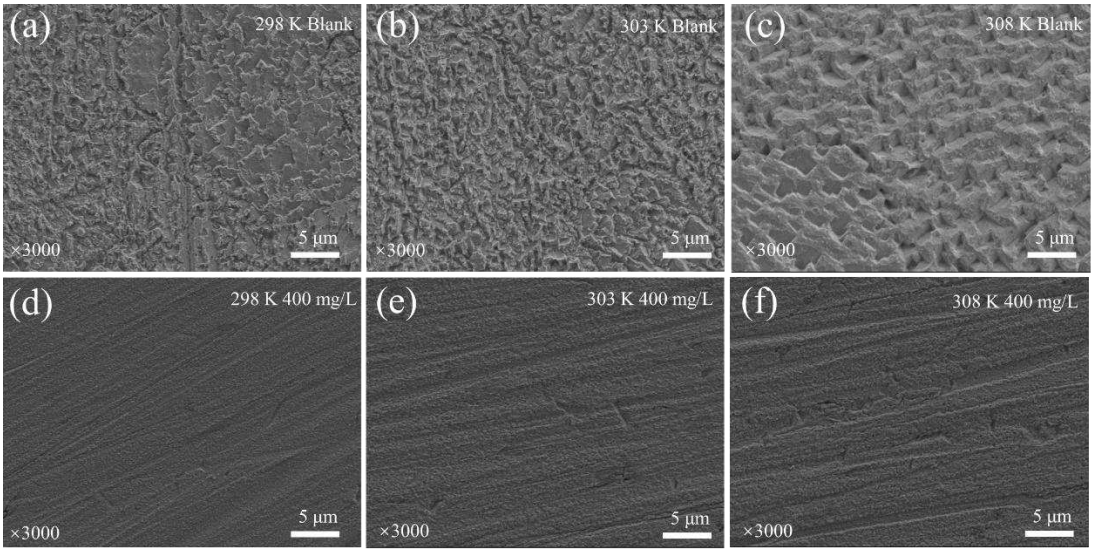
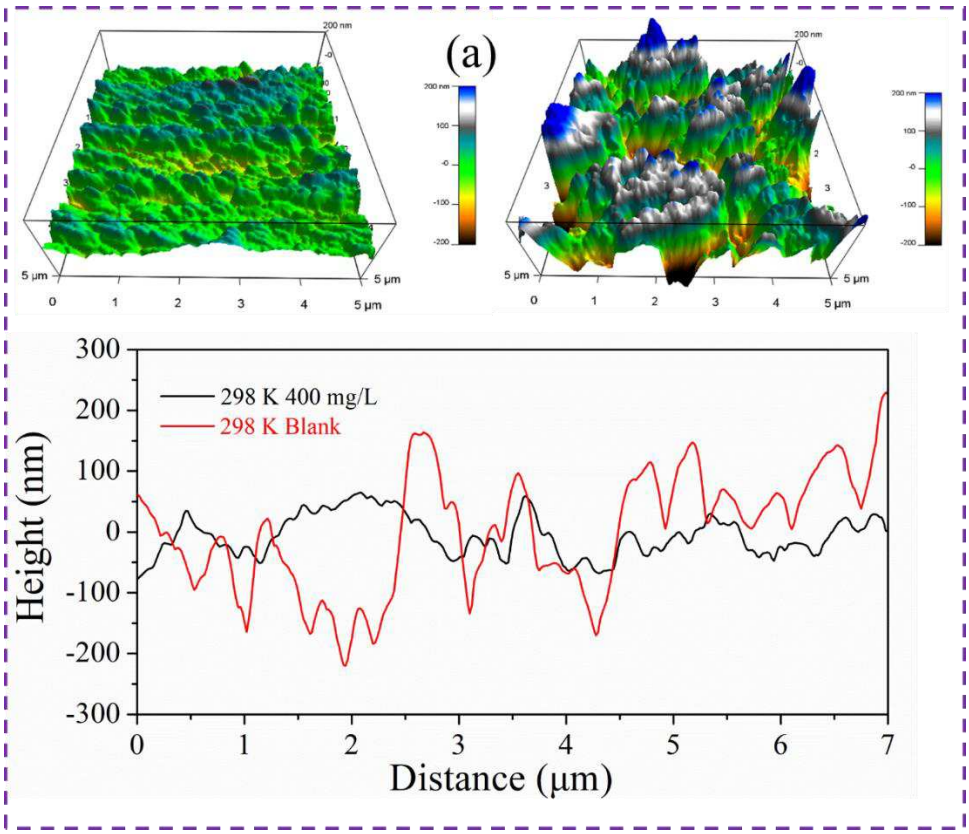
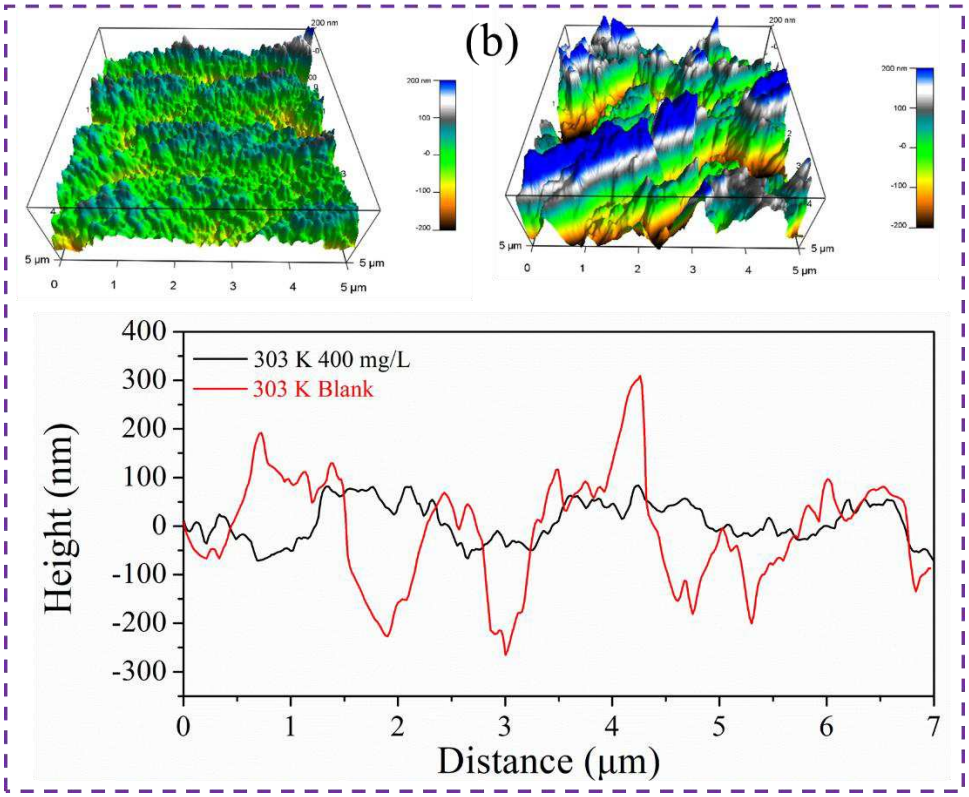


Fig. 5. SEM images illustrating the surface morphology of the copper–nickel alloy after immersion in 0.5 M H_2SO_4, taken without the inhibitor (a–c) and with 400 mg/L TLWE (d–f), at temperatures of 298, 303, and 308 K. 3.5: AFM evaluation.

According to Fig. 6, the 3D morphology and diagonal contour profiles indicate that in the absence of TLWE, the copper–nickel alloy exhibits average surface roughness values of 82.3 nm, 98.7 nm, and 121.8 nm, respectively. When 400 mg/L SLLLE was added, the average roughness was 31.7 nm, 38.9 nm, and 45.1 nm at 298 K, 303 K, and 308 K. Thus, the presence of TLWE significantly reduces the alloy's erosion when exposed to H_2SO_4 solution.


(a)
298 K 400 mg/L
298 K Blank
Height (nm)
Distance (μm)


(b)
303 K 400 mg/L
303 K Blank
Height (nm)
Distance (μm)

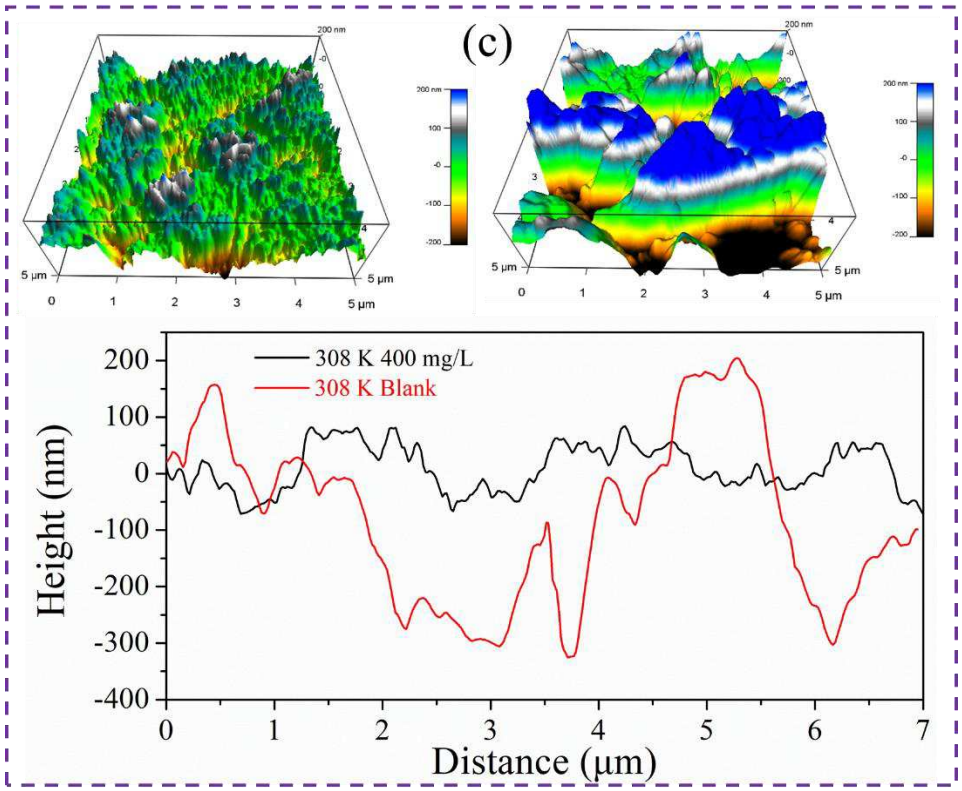


Fig. 6. Three-dimensional morphology and contour plots of the Cu-Ni alloy following 10 h immersion in 0.5 M H_2SO_4, both with and without 400 mg/L TLWE: (a) 298 K, (b) 303 K, and (c) 308 K

3.6 Electrochemical analysis

Fig. 7(b) clearly shows that the corrosion current density increases with rising temperature, highlighting the temperature-dependent effect, thereby intensifying Cu erosion. The Nyquist plot in Fig. 7(c) shows that the curve features both a capacitive arc and Warburg impedance. It is not without significance that the semicircle at high frequency reflects the charge transfer resistance, while the Warburg impedance originates from copper ion diffusion into the electrolyte after acid-induced corrosion. Moreover, the decrease in the radius of the capacitive semicircle with temperature rising from 298 K to 308 K signifies an intensified corrosive effect of the acidic

environment on the copper electrode.

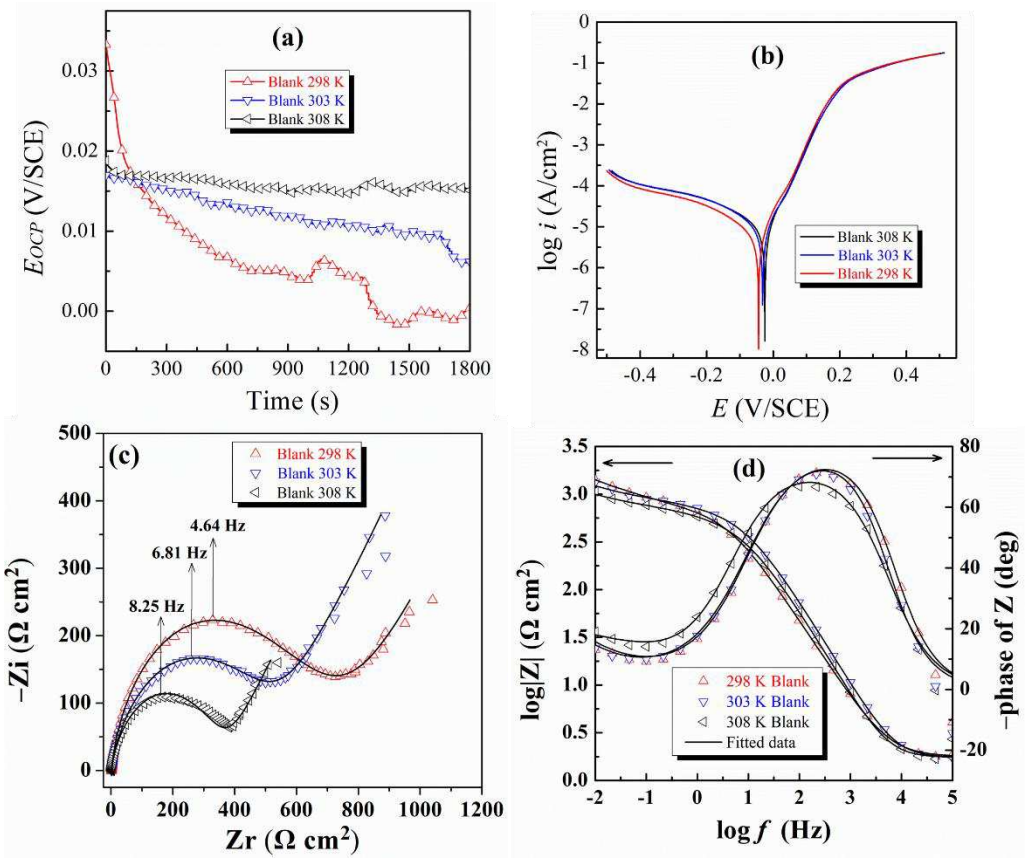


Fig. 7. (a) OCP, (b) polarization curve, (c) Nyquist plot, and (d) Bode plot of a copper-nickel alloy after immersion in 0.5 M H_2SO_4 without TLWE.

Fig. 8(b) demonstrates that the corrosion current density increases only slightly as the temperature increases, as indicated by the polarization curves, with minimal change in the capacitive arc radius, suggesting that TLWE, adsorbed on the Cu surface, effectively suppresses copper erosion within a certain temperature window, the erosion suppression protective film can still maintain its integrity. Moreover, the significant disappearance of Warburg impedance further confirms that TLWE efficiently suppresses copper corrosion after adsorption.

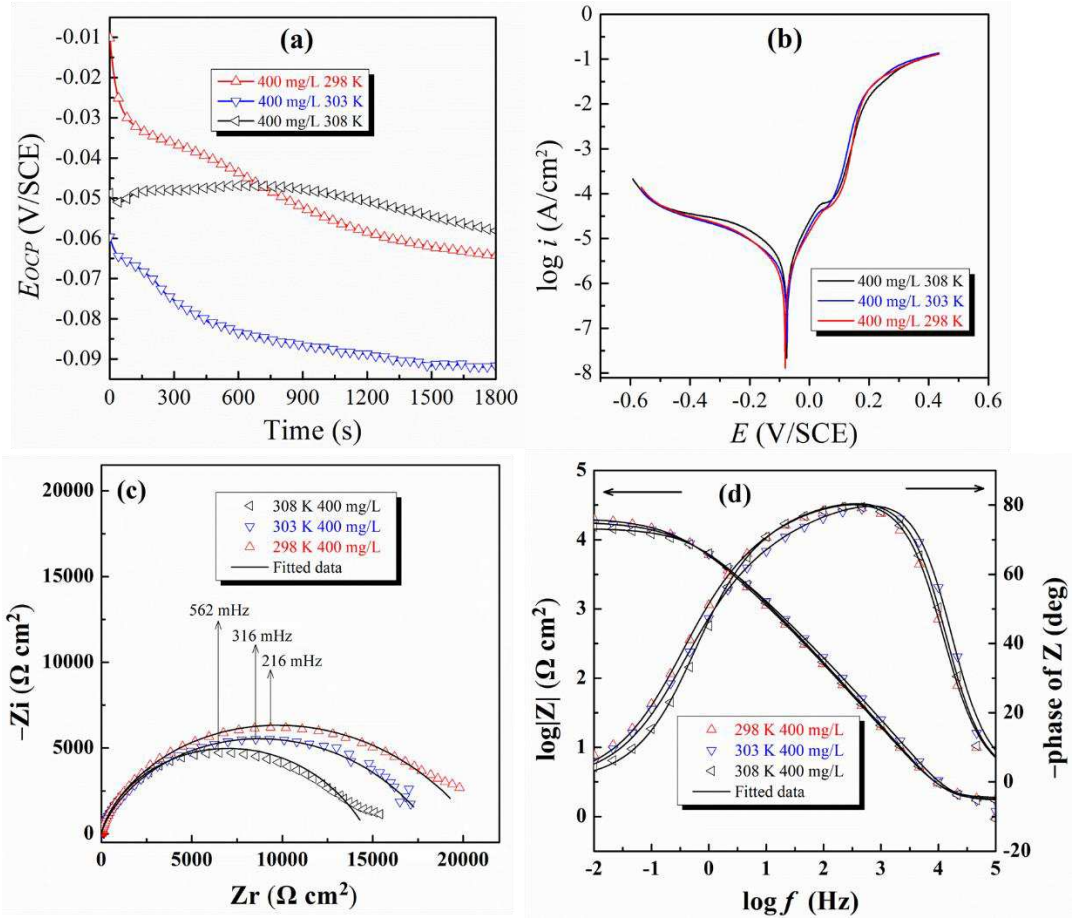


Fig. 8. (a) OCP, (b) polarization curve, (c) Nyquist diagram, and (d) Bode plot of a copper-nickel alloy dipped in H_2SO_4 supplemented with 400 mg/L TLWE at varying temperatures.

To quantitatively evaluate the temperature-dependent stability of TLWE corrosion inhibition performance. Table 1 displays the fitted data, where the erosion inhibition efficiency formula as follows [25-40]:

$$\eta(\%) = \frac{i_{corr,0} - i_{corr}}{i_{corr,0}} \times 100 \quad (3)$$

Table 1 shows that the corrosion inhibition efficiencies are 98.3%, 97.1% and 96.3% at 298, 303 and 308 K, separately. To evaluate temperature-dependent performance, these results demonstrate that TLWE maintains high corrosion inhibition efficiency within a specific range. By fitting the EIS spectra using the

equivalent circuit presented in Fig. 10, the corresponding parameters were obtained and compiled in Table 2, which also includes the expression for calculating inhibition efficiency [41-49]:

$$\eta(\%) = \frac{R_P - R_{P,0}}{R_p} \times 100 \quad (4)$$

Table 2 shows that corrosion inhibition efficiency remains around 95% even as temperature rises, demonstrating that TLWE forms a stable, dense protective film on the alloy.

Table 1. Tafel curves were recorded for the copper-nickel alloy electrode in H_2SO_4 with and without 400 mg/L TLWE at various temperatures.

T (K)	C (mg/L)	E_{corr}(mV/SCE)	i_{corr}(μA cm^{-2})	β_c(mV dec^{-1})	β_a(mV dec^{-1})	η(%)
298	0	–56	18.56	–195.2	79.4	—
	400	–94	0.32	–161.9	96.5	98.3
303	0	–47	22.17	–168.0	68.8	—
	400	–92	0.64	–154.6	62.8	97.1
308	0	–44	25.83	–184.2	97.9	—
	400	–87	0.95	–152.7	90.8	96.3

Table 2. EIS parameters of alloy dipped in 0.5 M H_2SO_4 without or with TLWE.

T	C	R_f	R_{ct}	R_p	C_f	n_1	C_{dl}	n_2	W	η (%)
(K)	(mg/L)	(kΩ cm^2)	(kΩ cm^2)	(kΩ cm^2)	(μF cm^{-2})		(μF cm^{-2})		(×10^{-2} Ω cm^2 s$^{1/2}$)	
298	0	0	0.76	0.76	156.4	0.82	177.9	0.51	15.2	—
	400	0.14	20.18	20.32	43.4	0.96	41.9	0. 78	—	96.2
303	0	0	0.65	0.65	167.8	0.96	184.6	0.58	10.9	—
	400	0.12	16.38	16.50	49.5	0.95	62.4	0.62	—	96.0
308	0	0	0.56	0.56	176.6	0.97	188.6	0.56	7.9	—
	400	0.08	13.72	13.80	55.4	0.97	68.1	0.65	—	95.9

As shown in Fig. 9(a), the OCP obviously tended to be stable after dipping the alloy in H_2SO_4 for 1800 seconds, suggesting that the alloy surface attained a transient steady state. The Tafel curves at different concentrations are presented in Fig. 9(b). A considerable reduction in corrosion current density is observed as the concentration of TLWE increases, owing to the formation of a tightly bound and uniform protective layer on the alloy surface. In addition, after adding TLWE, the cathode branch clearly showed a parallel trend, which indicates that TLWE failed to change the cathode mechanism of action, namely the reduction of oxygen, after adsorbing on the alloy surface, while the polarization curve of anode branch changed significantly, indicating that TLWE adsorption on the alloy efficient prevents the dissolution of copper ions. It is not without significance that Fig. 9(c) displays the Nyquist plots of TLWE at various concentrations on the copper-nickel alloy in H_2SO_4. As TLWE concentration rises, the capacitive reactance arc radius notably increases, showing that TLWE adsorption on copper-nickel alloy surfaces effectively hinders charge transfer. To illustrate the effect of concentration, Fig. 9(d) presents the Bode plots of TLWE. The experimental data clearly demonstrate that increasing concentration leads to significant growth in both impedance modulus and phase angle, strongly indicating that TLWE effectively inhibit corrosion on copper-nickel alloys.

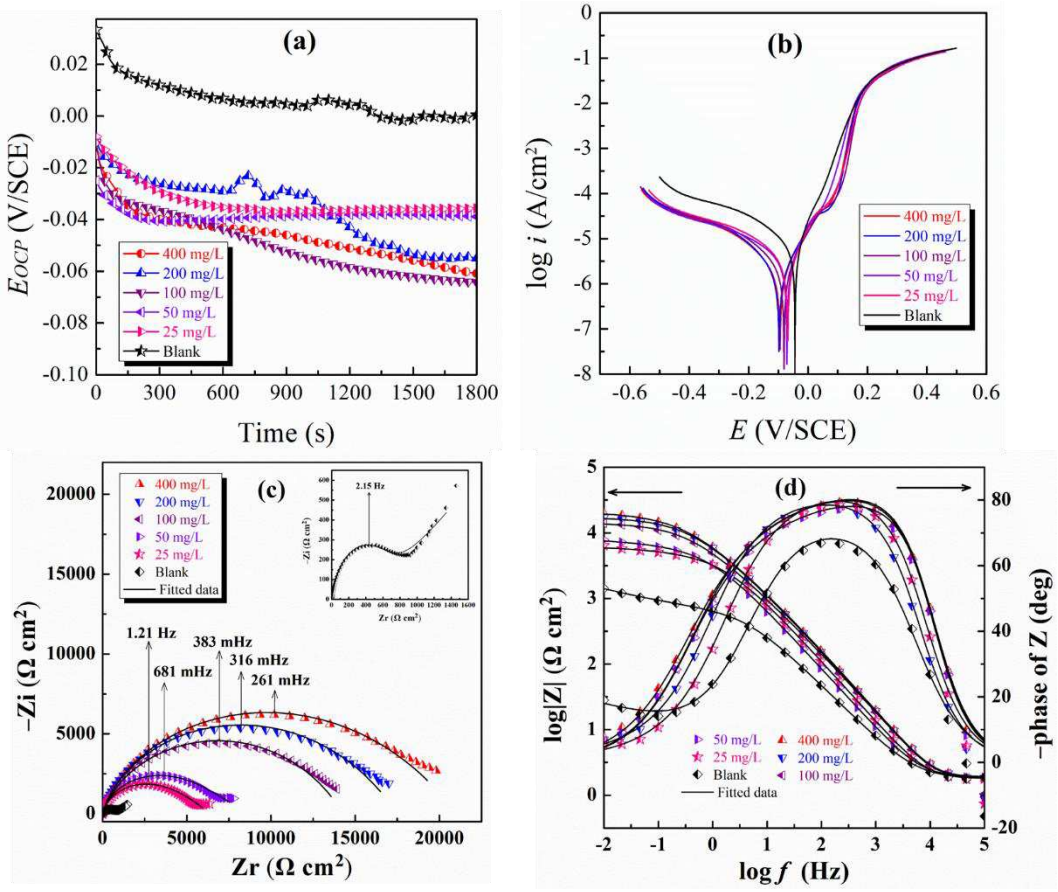


Fig. 9. (a) OCP, (b) polarization curve, (c) Nyquist plot, and (d) Bode plot of a copper-nickel alloy immersed in H_2SO_4 solution supplemented with 400 mg/L TLWE.

To quantitatively assess the effect of TLWE concentration on copper-nickel alloy, both polarization curves and EIS results were fitted, with the corresponding data shown in Table 3 and Table 4, respectively. It is not without significance that, as presented in Table 3, TLWE exhibits mixed-type inhibitory behavior, causing a drop in corrosion potential by more than 85 mV compared to the blank solution. At 400 mg/L, the corrosion current density drops from 18.56 to 0.32 μA cm^{-2}, corresponding to an inhibition efficiency of 98.3% in 0.5 M H_2SO_4. For the purpose of clarifying the EIS fitting parameters, Table 4 presents R_s as solution resistance, R_{ct} as charge transfer resistance, R_f as film resistance, Was Warburg impedance, and CPE as the constant

phase element [50-61]:

$$Z_{CPE} = \frac{1}{Y_0(j\omega)^n} \tag{5}$$

$$C = Y_0(\omega)^{n-1} = Y_0(2\pi f_{Z_{im-Max}})^{n-1} \tag{6}$$

After TLWE addition, C_{dl} and C_f demonstrated a marked decrease, as illustrated and explained through the following formula:

$$C_{dl} = \frac{\varepsilon^0 \varepsilon}{d} S \tag{7}$$

$$C_f = \frac{F^2 S}{4RT} \tag{8}$$

Utilized in the subsequent calculations, the parameters S and d, corresponding to the copper-nickel alloy area and the double-layer capacitor thickness respectively, reflect the system's electrochemical properties. With the alloy surface water molecules being replaced by the TLWE, the C_{dl} thickness increases while the effective alloy area decreases. It cannot be denied that C_f and C_{dl} do not follow a clear downward trend. Nor is it the case that the progressive replacement of water molecules by TLWE on the alloy does not lead to a more pronounced decrease in C_f and C_{dl}.

Table 3. Tafel curve data of alloy dipped in H_2SO_4 without and with varying concentrations of TLWE.

C (mg/L)	E_{corr}(mV/SCE)	i_{corr}(μA cm^{-2})	β_c(mV dec^{-1})	β_a(mV dec^{-1})	η(%)
Blank	−56	18.56	−195.1	79.4	—
25	−68	1.84	−181.6	74.1	90.1
50	−71	1.15	−172.3	81.6	93.8
100	−81	0.65	−163.1	93.1	96.5
200	−98	0.55	−157.6	85.8	97.0
400	−94	0.32	−161.9	96.5	98.3

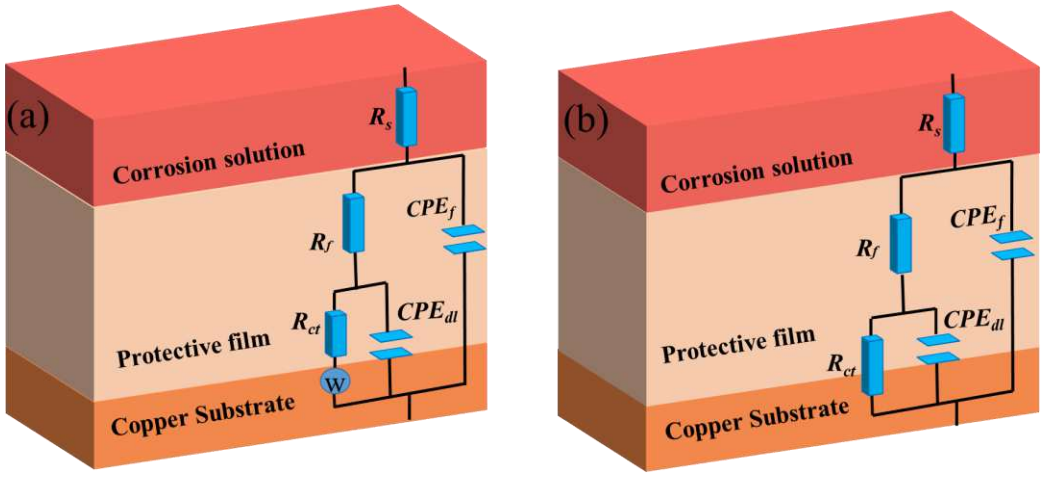


Fig. 10. The equivalent circuit for the copper-nickel alloy electrode in 0.5 M H_2SO_4 with and without TLWE: (a) featuring Warburg impedance, (b) without Warburg impedance. Table 4 presents the EIS parameters of the copper-nickel alloy electrode immersed in 0.5 M H_2SO_4 with and without TLWE.

Table 4. EIS parameters of the copper-nickel alloy electrode immersed in 0.5 M H_2SO_4 without and with TLWE.

C (mg/L)	R_f (kΩ cm^2)	R_{ct} (kΩ cm^2)	R_p (kΩ cm^2)	C_f (μF cm^{-2})	n_1	C_{dl} (μF cm^{-2})	n_2	W (×10^{-2} Ω cm^2 s$^{1/2}$)	η (%)
Blank	0	0.76	0.76	156.4	0.82	177.9	0.51	15.2	—
25	0.01	6.46	6.47	97.6	0.89	99.8	0.94	—	88.2
50	0.03	8.76	8.79	89.3	0.51	84.6	0.91	—	91.4
100	0.08	14.23	14.31	71.6	1	72.8	0.69	—	94.7
200	0.11	17.42	17.53	68.6	0.97	69.1	0.62	—	95.7
400	0.14	20.18	20.32	43.4	0.96	41.9	0.78	—	96.2

3.7 Adsorption isotherm model study

To evaluate the adsorption characteristics of TLWE on the alloy, electrochemical impedance spectroscopy (EIS) data were modeled employing multiple adsorption isotherms, specifically the Langmuir and Temkin frameworks, to elucidate the

adsorption mechanisms at the interface. The fitting results are displayed in Figs. 11 and 12. The following are the expressions of the isothermal adsorption equations [62-66]:

Langmuir isotherm: $$\frac{C}{\theta}=\frac{1}{K_{ads}}+C \tag{9}$$

Temkin adsorption isotherm: $$\exp^{(-2\alpha\theta)}=KC \tag{10}$$

El-Awady adsorption isotherm: $$\ln\frac{\theta}{1-\theta}=y\ln C+\ln K' \tag{11}$$

Frumkin adsorption isotherm: $$\ln\left[\frac{\theta}{(1-\theta)C}\right]=\ln K+2\alpha\theta \tag{12}$$

Based on the linear regression coefficients derived from the fitting results, the adsorption of TLWE is described by the Langmuir monolayer model. Furthermore, the Gibbs free energy for TLWE adsorption on the copper–nickel alloy was determined using Equation 13 [67-70]:

$$K_{ads}=\frac{1}{55.5}\exp(-\frac{\Delta G^{0}_{ads}}{RT}) \tag{13}$$

Exceeding 40 kJ/mol in magnitude, the observed data suggest that TLWE molecules coordinate with copper via electron sharing or transfer.

Falling below 20 kJ/mol in absolute adsorption energy, this condition indicates, this signifies that the TLWE and Cu-Ni alloy primarily exhibit van der Waals or electrostatic interactions characteristic of physical adsorption. Residing within the -20 to -40 kJ/mol range, the energy value suggests, the system demonstrates coexisting physical and chemical bonding mechanisms [71]. Consequently, the adsorption process at the TLWE and copper interface operates through a hybrid mechanism

combining both interaction types.

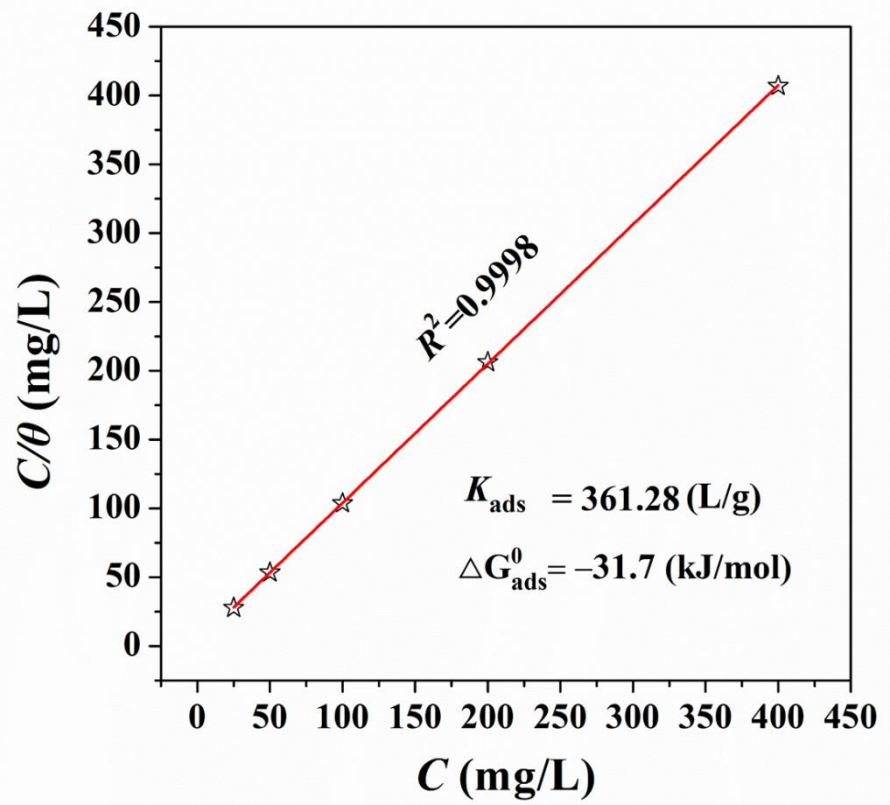


Fig. 11. The adsorption behaviour of TLWE on the Cu-Ni alloy.

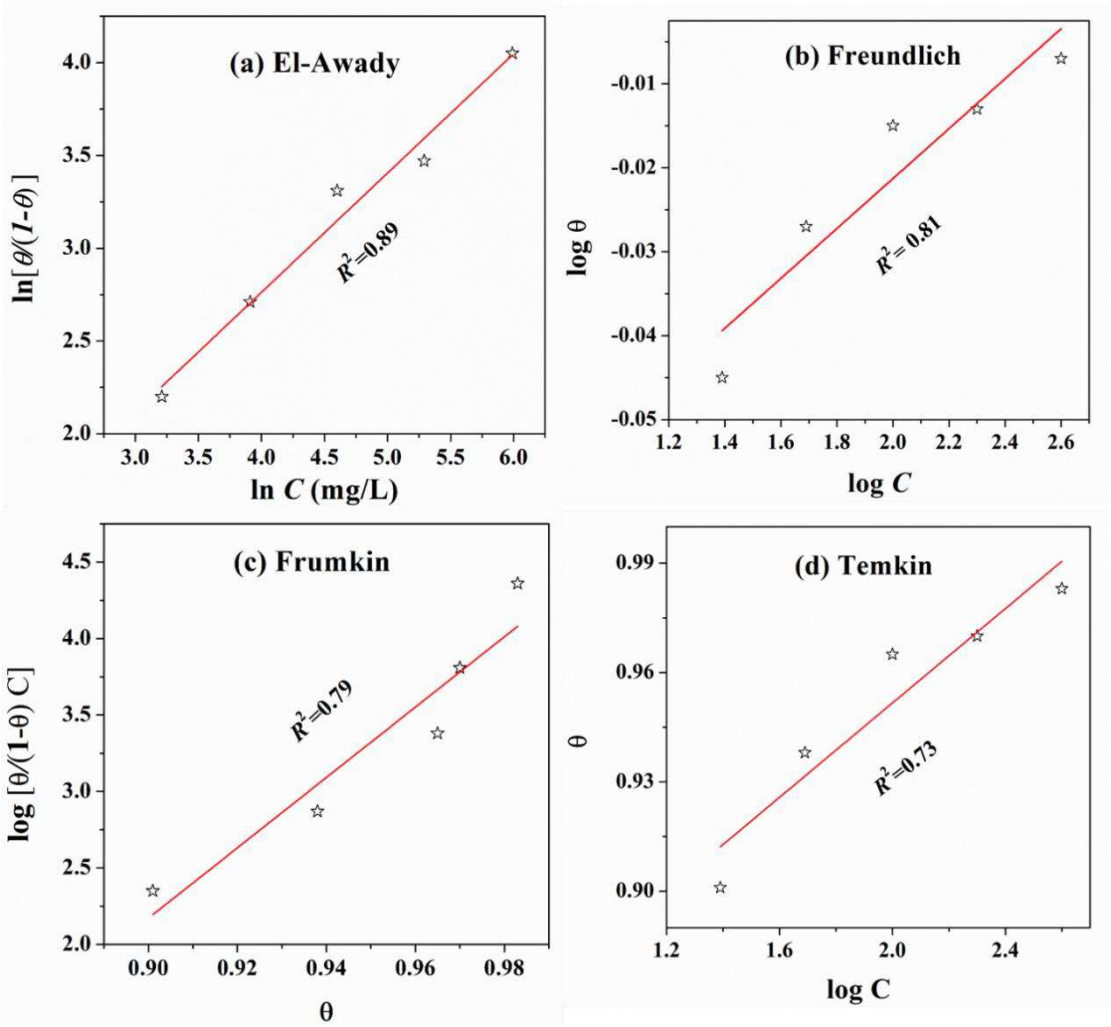


Fig. 12. Adsorption isotherms of TLWE on Cu-Ni alloy.

3.8 Adsorption mechanism investigation

Illustrating the proposed adsorption mechanism of TLWE on copper (Fig. 13), the study shows via electrochemical analysis that the extract primarily inhibits corrosion through a cathodic mechanism. Isotherm model fitting indicates that its adsorption follows the Langmuir monolayer model.

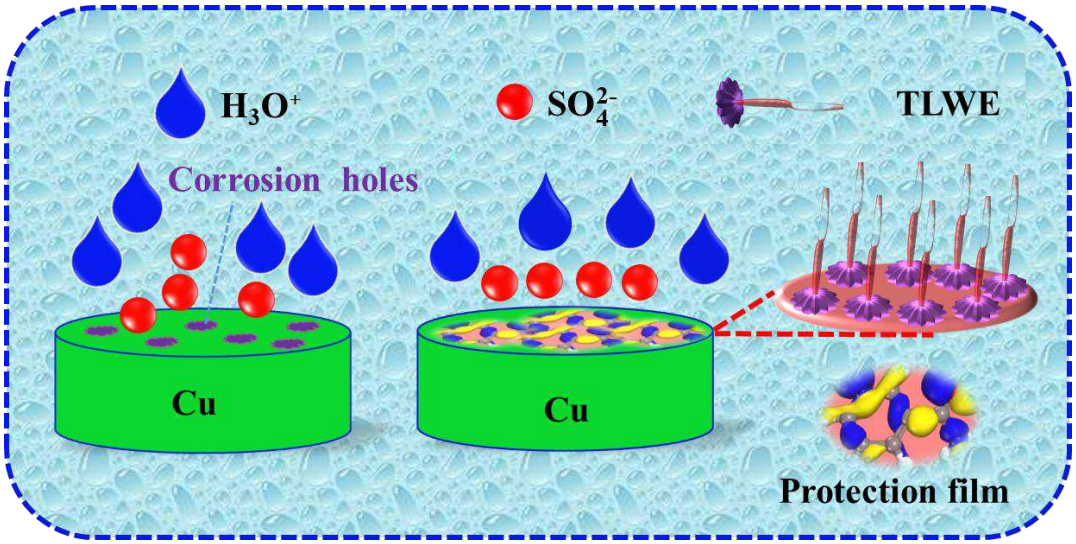


Fig. 13. Adsorption mechanism of TLWE on copper-nickel alloy.

4. Conclusion

1. Electrochemical tests confirm that TLWE effectively inhibits copper corrosion in H_2SO_4 medium, achieving a corrosion inhibition rate of >97%, which remains >95% even with increasing temperature.

2. Theoretical calculations confirm that the active components of TLWE have good anti-corrosion ability.

3. Surface morphology studies show that after TLWE is adsorbed on Cu, the degree of erosion reduces apparently.

4. The adsorption behavior is consistent with the Langmuir monolayer framework, encompassing a synergistic mechanism of physical and chemical adsorption.

Acknowledgement:

The authors extend their appreciation to Princess Nourah bint Abdulrahman University Researchers Supporting Project number (PNURSP2026R891), Princess Nourah bint Abdulrahman University, Riyadh, Saudi Arabia. The Ongoing Research

Funding program Project number (ORF-2026-381), King Saud University, Riyadh, Saudi Arabia. The joint fund project of Bijie science and technology ([2025] No.143).

Author contributions

Zhili Gong: Experiment, Theoretical calculation, Investigation, Writing - Original Draft.

Lei Guo: Methodology, Experiment design, Formal analysis, Writing - Review & Editing

Xin Li: Formal analysis, Visualization Software.

Naifa Alenazi: Supervision, Visualization Software

Abeer A. AlObaid: Supervision, Methodology

Funding

Not applicable.

Availability of data and materials

All data generated or analysed during this study are included in this published Article.

Declarations

Ethics approval and consent to participate

Not applicable.

Consent for publication

Not applicable.

Competing interests

The authors declare that there is no conflict of interest.

Reference

[1] B. Tan, Y. Liu, H. Ren, Z. Gong, X. Li, W. Li, L. Guo, R. Chen, J. Wei, Q. Dai, A.A. AlObaid, N, S-carbon quantum dots as inhibitor in pickling process of heat exchangers for enhanced performance in multi-stage flash seawater desalination, Desalination 589 (2024) 117969.

[2] M.M. Solomon, S.A. Umoren, N.M. Solomon, B. Durodola, A.Y. Adesina, P. Hall, M.O. Osundiya, Elucidating the corrosion characteristics of brine heater and evaporator condenser alloys during acid cleaning of MSF plants and its mitigation, Desalination 569 (2024) 117027.

[3] I.B. Onyeachu, M.M. Solomon, S.A. Umoren, I.B. Obot, A.A. Sorour, Corrosion inhibition effect of a benzimidazole derivative on heat exchanger tubing materials during acid cleaning of multistage flash desalination plants, Desalination 479 (2020) 114283.

[4] Y.S. Taha, M. Nasr-Esfahani, Synergistic corrosion inhibition of propargyl alcohol and Schiff base on the corrosion of mild steel in hot HCl solution, New Journal of Chemistry 50(6) (2026) 2904-2915.

[5] B. Tan, H. Ren, Y. Liu, X. Li, R. Wang, J. Sun, X. Cao, Q. Dai, L. Guo, H. Liu, M.K. Al-Sadoon, Insight into the anti-corrosion performance of crop waste as a degradable corrosion inhibitor for copper in sulfuric acid medium, Industrial Crops and Products 222 (2024) 119654.

[6] A.H.E. Moustafa, H.H. Abdel-Rahman, M. Hagar, S.A.A. Bishr, A multi-faceted study combining quantum chemical, Hammett parameters, and antibacterial assessment for imidazole: based green ionic liquids corrosion inhibition, BMC Chemistry 20(1) (2026) 89.

[7] M.A. Ahmed, S. Amin, A.A. Mohamed, Current and emerging trends of inorganic, organic and eco-friendly corrosion inhibitors, RSC Adv 14(43) (2024) 31877-31920.

[8] A. Zhang, X. Li, Y. Chen, C. Cao, C. Shi, J. Liu, Effects of hydroxyl and trifluoromethyl substituents on the corrosion inhibition of benzotriazole derivatives in copper surface planarization, New Journal of Chemistry 50(1) (2026) 24-28.

[9] A. Sharma, A. Saxena, J. Kaur, G.V. Rambabu, R. C, A.A. Lakshmi, A. Sharma, A. Kumar, R. Tyagi, Mixture of Rubia cordifolia and KI as an efficient corrosion inhibitor for steel in 3.5% NaCl: electrochemical and surface studies of steel, Chemical Physics Impact 12 (2026) 100983.

[10] A.H. Jabbar, S.M.H. Kamona, S.K. Abbood, T.K. Hussein, D.N. Al-Saidi, S.M. Hameed, R.A.K. Rashid, H.A. Abbas, M.M. Kadhim, The effective and sustainable application of a green amino acid-based corrosion Inhibitor for Cu metal, Chemical Physics Impact 7 (2023) 100316.

[11] H.M.K. Sheit, K.S. Mohan, K.V. Gunavathy, S.S. Syed abuthahir, M.V. Mohamed, P. Subhapriya, A. Samsathbegum, G.H. Sindhuja, Investigation on the corrosion inhibition efficiency of 2, 4-diphenyl-3-aza bicyclo[3.3.1] nonan-9-one in carbon steel immersed in acidic media, Chemical Physics Impact 8 (2024) 100521.

[12] R. Aslam, Q. Wang, Y. Sun, C. Verma, A. Alfantazi, Z. Yan, Functionalized metal–organic frameworks for sustainable corrosion protection of carbon steel: interfacial chemistry and mechanistic insights, New Journal of Chemistry 50(5) (2026) 2417-2432.

[13] M. Khnifira, W. Boumya, J. Attarki, A. Mahsoune, M. Sadiq, M. Abdennouri, S. Kaya, N. Barka, A combined DFT, Monte Carlo, and MD simulations of adsorption study of heavy metals on the carbon graphite (111) surface, Chemical Physics Impact 5 (2022) 100121.

[14] A. Fonseca, L. Gutierrez Pua, A.M. Miranda, F. Hernandez-Tenorio, A.A. Saez, Y. Pineda Triana, Integrated framework for designing durable green corrosion inhibitors from Spirulina: Cultivation, extraction, and electrochemical evaluation, iScience 29(4) (2026) 115220.

[15] X. Wen, Y. Chen, F. Zhu, X. Li, H. Lin, W. Jiang, Molecular dynamics simulation and

experimental study of electrochemical dissolution properties of 440C stainless steel, iScience 28(11) (2025) 113845.
[16] Y. Feng, B. Zhou, M.J. Wang, K. Xu, Y. Cheng, Z. Song, Investigating the corrosion inhibition mechanism of Eucalyptus citriodora leaf extract on Q235 carbon steel, iScience 28(11) (2025) 113655.
[17] G. Huang, W. Chen, C. Miao, C. Shen, Y.b. Wang, G.A. Zhang, A novel high-efficient imidazoline derivative corrosion inhibitor for carbon steel in CO2-containing oilfield produced water: experimental and theoretical studies, BMC Chemistry 19(1) (2025) 234.
[18] B. Tan, H. Ren, C. Yin, X. Li, X. Li, R. Wang, L. Guo, Y. Zhang, M.K. Al-Sadoon, Nepeta cataria L. leaf extracts as eco-conscious corrosion inhibitor for copper in H2SO4 medium, Colloids and Surfaces A: Physicochemical and Engineering Aspects 711 (2025) 136399.
[19] Z. Gong, R. Zhang, L. Guo, R. Marzouki, Pine needle extract as inhibitor in heat exchanger pickling process to improve the performance of multi-stage flash desalination, Desalination 613 (2025) 119073.
[20] H. Huang, L. Xie, X. Chen, W. Li, M.K. Al-Sadoon, Insight into anti-corrosion mechanism of Zingiber officinale Roscoe leaf extract as inhibitor, Materials Today Communications 43 (2025) 111702.
[21] K. Helmja, M. Vaher, T. Pussa, P. Raudsepp, M. Kaljurand, Evaluation of antioxidative capability of the tomato (Solanum lycopersicum) skin constituents by capillary electrophoresis and high-performance liquid chromatography, Electrophoresis 29(19) (2008) 3980-3988.
[22] K. Helmja, M. Vaher, J. Gorbatšova, M. Kaljurand, Characterization of bioactive compounds contained in vegetables of the Solanaceae family by capillary electrophoresis, Proc. Estonian Acad. Sci. Chem. 56 (2007) 172–186.
[23] B. Tan, Y. Liu, Z. Gong, X. Zhang, J. Chen, L. Guo, J. Xiong, J. Liu, R. Marzouki, W. Li, Pyracantha fortuneana alcohol extracts as biodegradable corrosion inhibitors for copper in H2SO4 media, Journal of Molecular Liquids 397 (2024) 124117.
[24] W. Daoudi, B. El Ibrahimi, O. Dagdag, E. Berdimurodov, L. Guo, E.E. Ebenso, A. Oussaid, A. El Aatiaoui, New chlorophenyl-imidazole derivative as a novel corrosion inhibitor in the gas and oil industry, Journal of Physics and Chemistry of Solids 179 (2023) 111409.
[25] B. Tan, Z. Gong, W. He, J. Xiong, L. Guo, R. Marzouki, Insight into the anti-corrosion mechanism of crop waste Arachis hypogaea L. leaf extract for copper in sulfuric acid medium, Sustainable Chemistry and Pharmacy 38 (2024) 101449.
[26] H. Ren, Y. Liu, Z. Gong, B. Tan, H. Deng, J. Xiong, P. Shao, Q. Dai, J. Cao, R. Marzouki, Pumpkin Leaf Extract Crop Waste as a New Degradable and Environmentally Friendly Corrosion Inhibitor, Langmuir 40(11) (2024) 5738-5752.
[27] S. Wan, T. Zhang, H. Chen, B. Liao, X. Guo, Kapok leaves extract and synergistic iodide as novel effective corrosion inhibitors for Q235 carbon steel in H2SO4 medium, Industrial Crops and Products 178 (2022) 114649.
[28] J. Lazrak, E. Ech-chihbi, B. El Ibrahimi, F. El Hajjaji, Z. Rais, M. Tachihante, M. Taleb, Detailed DFT/MD simulation, surface analysis and electrochemical computer explorations of aldehyde derivatives for mild steel in 1.0 M HCl, Colloids and Surfaces A: Physicochemical and Engineering Aspects 632 (2022) 127822.
[29] B. El Ibrahimi, A. Baddouh, R. Oukhrib, S. El Issami, Z. Hafidi, L. Bazzi, Electrochemical and in silico investigations into the corrosion inhibition of cyclic amino acids on tin metal in the saline environment, Surfaces and Interfaces 23 (2021) 100966.

[30] R.N. Felaly, M. Alfakeer, A.A.I. Ali, S.S. Al-Juaid, E.M. Mabrouk, A.Y. El-Etre, D.F. Seyam, M. Abdallah, Enhanced corrosion protection of copper alloy in 2.0 M HNO3 solution using expired solo sept, slim-lax and well derm drugs, International Journal of Electrochemical Science 19(8) (2024) 100657.
[31] S. de Carvalho Mendes Lopes, L.M. de Souza, E.C. Pereira, A.O. Gadioli, S.N. Monteiro, A.R.G. Azevedo, Evaluation of the efficiency of 1-ethyl-3-methylimidazolium chloride ionic liquid as corrosion inhibitor for the welded duplex stainless steel in acid environment, Journal of Materials Research and Technology 35 (2025) 5614-5628.
[32] C. Li, Z. Wang, B. Liu, S. Wang, H. Xie, L. Zhang, H. Du, Y. Zhang, Corrosion inhibition mechanism of Na2CrO4 on 316L in highly concentrated NaOH solutions, Journal of Materials Research and Technology 35 (2025) 4792-4804.
[33] C. Sang, J. Qiu, B. Yuan, K. Zhang, N. Huang, Q. Wang, H. Ma, L. Li, C. Wang, Inhibition mechanism of self-assembled epoxy-silane/dithiol film on copper corrosion, Journal of Materials Research and Technology 35 (2025) 1941-1949.
[34] J.-h. Zhu, B.-l. Lin, T.-h. Duan, H.-q. Lin, G.-y. Zhang, X.-x. Zhou, Y.-y. Xu, Zea mays bracts extract as an eco-friendly corrosion inhibitor for steel in HCl pickling solution: Experimental and simulation studies, Arabian Journal of Chemistry 17(9) (2024) 105895.
[35] L. Zhao, F. Wang, X. Zhang, Y. Han, Y. Wang, Z. Yang, Z. Cao, Y. Wu, Y. Xu, Syntheses, properties and mechanistic studies of 8-aminooctanoic acid-modified polyaspartic acid polymers for calcium scale inhibition, Arabian Journal of Chemistry 17(4) (2024) 105717.
[36] A. Dehghani, B. Ramezanzadeh, Rosemary extract inhibitive behavior against mild steel corrosion in tempered 1 M HCl media, Industrial Crops and Products 193 (2023) 116183.
[37] A. Zarei, A. Dehghani, L. Guo, B. Ramezanzadeh, Pepper extract effectiveness as a natural inhibitor against corrosion of steel samples (SS) in 1 M hydrochloric acid; Theoretical (DFT calculation – MD simulation), thermodynamic, and electrochemical-surface studies, Industrial Crops and Products 189 (2022) 115839.
[38] K. Yang, H. Feng, N. Chen, J. Hou, M.M.Y. Modwi, J. Zhao, J. Wang, J. Qiu, Green synthesis of polydopamine-modified attapulgite: a sustainable solution for mitigating carbon steel corrosion in amino-sulfonic acid-laden environments, New Journal of Chemistry 49(22) (2025) 9256-9266.
[39] M. Alsarrani, S.A.M. Ali, M.A.A. Mahmoud, H.A. El Nagy, A.Z. Ibrahim, A.M. Ali, M.A. Sayed, A.F. El-kott, K. Al-Ghamdi, M.E. Salem, M. Al-Abyadh, Synthesis and characterizations of 4,6-dihydroxyisophthalohydrazide derivative for mitigation corrosion inhibition of low carbon steel in acidic medium, BMC Chemistry 20(1) (2025) 6.
[40] Z.A.M. Al-Ahmed, M.M. Kamel, M.A.A. Mahmoud, S.A.M. Ali, A.Z. Ibrahim, B.M. Alshehri, 4-amino-5-(trifluoromethyl)-4H-1, 2, 4-triazole-3-thiol as an effective corrosion inhibitor for low carbon steel in HCl environment: experimental and theoretical studies, BMC Chemistry 19(1) (2025) 205.
[41] I. Merimi, R. Aslam, B. Hammouti, T. Szumiata, H. Lgaz, I.-M. Chung, Adsorption and inhibition mechanism of (Z)-4-((4-methoxybenzylidene)amino)-5-methyl-2,4-dihydro-3H-1,2,4-triazole-3-thione on carbon steel corrosion in HCl: Experimental and theoretical insights, Journal of Molecular Structure 1231 (2021) 129901.
[42] H. Lgaz, S.K. Saha, A. Chaouiki, K.S. Bhat, R. Salghi, Shubhalaxmi, P. Banerjee, I.H. Ali, M.I. Khan, I.-M. Chung, Exploring the potential role of pyrazoline derivatives in corrosion inhibition of mild steel in hydrochloric acid solution: Insights from experimental and computational studies,

Construction and Building Materials 233 (2020) 117320.
[43] H. Lgaz, S. Masroor, M. Chafiq, M. Damej, A. Brahmia, R. Salghi, M. Benmessaoud, I.H. Ali, M.M. Alghamdi, A. Chaouiki, I.-M. Chung, Evaluation of 2-Mercaptobenzimidazole Derivatives as Corrosion Inhibitors for Mild Steel in Hydrochloric Acid, Metals 10(3) (2020) 357.
[44] H. Lgaz, I.-M. Chung, M.R. Albayati, A. Chaouiki, R. Salghi, S.K. Mohamed, Improved corrosion resistance of mild steel in acidic solution by hydrazone derivatives: An experimental and computational study, Arabian Journal of Chemistry 13(1) (2020) 2934-2954.
[45] R. Solmaz, Y.A. Dursun, E.A. Şahin, İ.H. Gecibesler, M. Doğrubaş, M. Tunç, N. Çağlayan, İ. Şahin, İ. Dursun, S. Bayındır, İ.Y. Erdoğan, G. Kardaş, Bingöl propolis self-assembled monolayer films: Preparation, characterization and application as corrosion inhibitors for copper protection in NaCl environment, Materials Chemistry and Physics 315 (2024) 128956.
[46] R. Solmaz, A. Salcı, Y.A. Dursun, G. Kardaş, A comprehensive study on the adsorption, corrosion inhibition efficiency and stability of acriflavine on mild steel in 1 M HCl solution, Colloids and Surfaces A: Physicochemical and Engineering Aspects 674 (2023) 131908.
[47] X. Wang, Y. Lei, Z.N. Jiang, Q.H. Zhang, Y.Y. Li, H.F. Liu, G.A. Zhang, Developing two thiocarbohydrazide modified glucose derivatives as high-efficiency green corrosion inhibitors for carbon steel, Industrial Crops and Products 188 (2022) 115680.
[48] J. Wang, F. Seidi, Y. Huang, H. Xiao, Smart lignin-based polyurethane conjugated with corrosion inhibitor as bio-based anticorrosive sublayer coating, Industrial Crops and Products 188 (2022) 115719.
[49] H.A. Ali, A.A. El-Hossiany, A.S. Abousalem, M.A. Ismail, A.E.-A.S. Fouda, E.A. Ghaith, Synthesis of new binary trimethoxyphenylfuran pyrimidinones as proficient and sustainable corrosion inhibitors for carbon steel in acidic medium: experimental, surface morphology analysis, and theoretical studies, BMC Chemistry 18(1) (2024) 182.
[50] B. Tan, S. Zhang, X. Cao, A. Fu, L. Guo, R. Marzouki, W. Li, Insight into the anti-corrosion performance of two food flavors as eco-friendly and ultra-high performance inhibitors for copper in sulfuric acid medium, Journal of Colloid and Interface Science 609 (2022) 838-851.
[51] B. Tan, W. Lan, S. Zhang, H. Deng, Y. Qiang, A. Fu, Y. Ran, J. Xiong, R. Marzouki, W. Li, Passiflora edulia Sims leaves Extract as renewable and degradable inhibitor for copper in sulfuric acid solution, Colloids and Surfaces A: Physicochemical and Engineering Aspects 645 (2022) 128892.
[52] Y. El aoufir, S. Zehra, H. Lgaz, A. Chaouiki, H. Serrar, S. Kaya, R. Salghi, S.K. AbdelRaheem, S. Boukhris, A. Guenbour, I.-M. Chung, Evaluation of inhibitive and adsorption behavior of thiazole-4-carboxylates on mild steel corrosion in HCl, Colloids and Surfaces A: Physicochemical and Engineering Aspects 606 (2020) 125351.
[53] H. Lgaz, I.-M. Chung, R. Salghi, I.H. Ali, A. Chaouiki, Y. El Aoufir, M.I. Khan, On the understanding of the adsorption of Fenugreek gum on mild steel in an acidic medium: Insights from experimental and computational studies, Applied Surface Science 463 (2019) 647-658.
[54] L.M. Doubova, S. Rondinini, A. Vertova, L. Bulgariu, Studying electron transfer reaction at the Au/n-decanethiol/aqueous solution of NaNO3 interface by electrochemical impedance spectroscopy, Russian Journal of Electrochemistry 49(1) (2013) 26-37.
[55] A. Nazari, B. Ramezanzadeh, L. Guo, A. Dehghani, Application of green active bio-molecules from the aquatic extract of Mint leaves for steel corrosion control in hydrochloric acid (1M) solution: Surface, electrochemical, and theoretical explorations, Colloids and Surfaces A: Physicochemical and Engineering Aspects 656 (2023) 130540.
[56] A. Dehghani, A.H. Mostafatabar, B. Ramezanzadeh, Synergistic anticorrosion effect of Brassica

Hirta phytoconstituents and cerium ions on mild steel in saline media: Surface and electrochemical evaluations, Colloids and Surfaces A: Physicochemical and Engineering Aspects 656 (2023) 130503.
[57] M.A. Deyab, E. Guibal, Enhancement of corrosion resistance of the cooling systems in desalination plants by green inhibitor, Sci Rep 10(1) (2020) 4812.
[58] M.A. Deyab, S.S.A. El-Rehim, H.H. Hassan, A.M. Shaltot, Impact of rare earth compounds on corrosion of aluminum alloy (AA6061) in the marine water environment, Journal of Alloys and Compounds 820 (2020) 153428.
[59] M.A. Deyab, Enhancement of corrosion resistance in MSF desalination plants during acid cleaning operation by cationic surfactant, Desalination 456 (2019) 32-37.
[60] M. Yousefpour, R.z. Shayegh, A.H. Hafazeh, H. Tavakoli, Corrosion inhibition performance of carbon steel in sulfuric acid using gum arabic extract: experimental insights, DFT analysis, and molecular dynamics simulations, Results in Engineering 28 (2025) 107220.
[61] C.A. Igboamalu, V.I. Chukwuike, A. James, O. Akaranta, Green metal protection: Potency of ethanolic extracts of Lagenaria breviflora leaf as inhibitor for mild steel dissolution in 0.5M HCl medium, Results in Engineering 28 (2025) 107754.
[62] A.R. Shahmoradi, N. Talebibahmanbigloo, C. Nickhil, R. Nisha, A.A. Javidparvar, P. Ghahremani, G. Bahlakeh, B. Ramezanzadeh, Molecular-MD/atomic-DFT theoretical and experimental studies on the quince seed extract corrosion inhibition performance on the acidic-solution attack of mild-steel, Journal of Molecular Liquids 346 (2022) 117921.
[63] M.H. Shahini, M. Ramezanzadeh, B. Ramezanzadeh, G. Bahlakeh, The role of ethanolic extract of Stachys byzantina's leaves for effective decreasing the mild-steel (MS) degradation in the acidic solution; coupled theoretical/experimental assessments, Journal of Molecular Liquids 329 (2021) 115571.
[64] M.H. Shahini, M. Ramezanzadeh, G. Bahlakeh, B. Ramezanzadeh, Superior inhibition action of the Mish Gush (MG) leaves extract toward mild steel corrosion in HCl solution: Theoretical and electrochemical studies, Journal of Molecular Liquids 332 (2021) 115876.
[65] M.H. Shahini, M. Keramatinia, M. Ramezanzadeh, B. Ramezanzadeh, G. Bahlakeh, Combined atomic-scale/DFT-theoretical simulations & electrochemical assessments of the chamomile flower extract as a green corrosion inhibitor for mild steel in HCl solution, Journal of Molecular Liquids 342 (2021) 117570.
[66] O.O. Ekerenam, A.I. Ikeuba, C.N. Njoku, D.I. Njoku, W. Emori, I.K. Nwokolo, I.-I.N. Etim, B.O. Okonkwo, I.I. Udoh, E.F. Daniel, P.C. Uzoma, B.O. Awonusi, S.K. Kolawole, I.P. Etim, O.S. Olanrele, Advancements in corrosion studies and protective measures for copper and copper-based alloys in varied environmental conditions, Results in Engineering 26 (2025) 105257.
[67] H. Nady, A. Elgendy, W.A.A. Arafa, E.S. Gad, Insight into the inhibition performance of thiosemicarbazones as efficient inhibitors for copper in acidic environment: Combined experimental and computational investigations, Colloids and Surfaces A: Physicochemical and Engineering Aspects 647 (2022) 129208.
[68] K. Dahmani, M. Galai, M. Ouakki, A. Elgendy, R. Ez-Zriouli, R. Lachhab, S. Briche, M. Cherkaoui, Corrosion inhibition of copper in sulfuric acid via environmentally friendly inhibitor (Myrtus Communis): Combining experimental and theoretical methods, Journal of Molecular Liquids 347 (2022) 117982.
[69] H.E. Aadad, M. Galai, M. Ouakki, A. Elgendy, M.E. Touhami, A. Chahine, Improvement of the corrosion resistance of mild steel in sulfuric acid by new organic-inorganic hybrids of

Benzimidazole-Pyrophosphate: Facile synthesis, characterization, experimental and theoretical calculations (DFT and MC), Surfaces and Interfaces 24 (2021) 101084.
[70] A. Elgendy, H. Nady, M.M. El-Rabiei, A.A. Elhenawy, Understanding the adsorption performance of two glycine derivatives as novel and environmentally safe anti-corrosion agents for copper in chloride solutions: experimental, DFT, and MC studies, RSC Adv 9(72) (2019) 42120-42131.
[71] M. Abdallah, J.H. Al-Fahemi, K.A. Soliman, A.S. Al-Gorair, M.S. Al-Sharif, S.S. Al-Juaid, S. Abd El Wanees, M. Sobhi, Exploring cinnamon extract's potential as a green corrosion inhibitor for X65 carbon steel in sulfuric acid: a comprehensive investigation, Journal of Dispersion Science and Technology 1 (2024) 1-15.